



Stackable bipolar pouch cells with corrosion-resistant current collectors enable high-power aqueous electrochemical energy storage

Journal:	<i>Energy & Environmental Science</i>
Manuscript ID	EE-ART-02-2018-000546.R2
Article Type:	Paper
Date Submitted by the Author:	22-May-2018
Complete List of Authors:	Evanko, Brian; University of California Santa Barbara, Materials Department Yoo, Seung ; University of Santa Barbara, Department of Chemistry and Biochemistry Lipton, Jason; Yale University Chun, Sang-eun; Kyungpook National University, Moskovits, M; University of California, Department of Chemistry and Biochemistry 9510 Ji, Xiulei; Oregon State University, Department of Chemistry Boettcher, Shannon; University of Oregon, Stucky, Galen; University of California, Department of Chemistry and Biochemistry

Stackable bipolar pouch cells with corrosion-resistant current collectors enable high-power aqueous electrochemical energy storage

Brian Evanko,^{#ab} Seung Joon Yoo,^{*#b} Jason Lipton,^c Sang-Eun Chun,^d Martin Moskovits,^c Xiulei Ji,^e Shannon W. Boettcher,^{*f} and Galen D. Stucky^{ac}

^a *Materials Department, University of California, Santa Barbara, California 93106, USA*

^b *Materials Research Laboratory, University of California, Santa Barbara, California, 93106, USA. E-mail: sjyoo@chem.ucsb.edu*

^c *Department of Chemistry & Biochemistry, University of California, Santa Barbara, California 93106, USA*

^d *School of Materials Science and Engineering, Kyungpook National University, Daegu 41566, Republic of Korea*

^e *Department of Chemistry, Oregon State University, Corvallis, Oregon 97331, USA.*

^f *Department of Chemistry & Biochemistry, University of Oregon, Eugene, Oregon 97403, USA. E-mail: swb@uoregon.edu*

+ Electronic supplementary information (ESI) available: Materials, experimental details, Figures S1-S16, resistivity calculations, cost analysis, cell design/assembly, and electrochemical testing protocols. See DOI:

These authors contributed equally to this work.

ABSTRACT

A critical bottleneck in the development of aqueous electrochemical energy storage systems is the lack of viable complete cell designs. We report a metal-free, bipolar pouch cell designed with carbon black/polyethylene composite film (CBPE) current collectors as a practical cell architecture. The light-weight, corrosion-resistant CBPE provides stable operation in a variety of aqueous electrolytes over a ~ 2.5 V potential range. Because CBPE is heat-sealable, it serves simultaneously as both the pouch cell packaging and seal in addition to its use as a current collector. Although this non-metallic composite has a low electrical conductivity relative to

metal foils, current travels only a short distance in the through-plane direction of the current collector in the bipolar cell configuration. This shorter path length lowers the effective electrical resistance, making the design suitable for high-power applications. We test the cell architecture using an aqueous ZnBr_2 battery chemistry and incorporate tetrabutylammonium cations to improve the intrinsic low Coulombic efficiency and fast self-discharge of non-flow ZnBr_2 cells. These devices demonstrate a cell-level energy density of 50 W h L^{-1} at a 10 C rate (0.5 kW L^{-1}), with less than 1% capacity loss over 500 cycles. A large-area ($> 6 \text{ cm}^2$) 4-cell stack is built to illustrate that the pouch cells are scalable to practical dimensions and stackable without sacrificing performance. The device operates in the range of 5-7 V and has an internal self-balancing mechanism that prevents any individual cell in the stack from overcharging. The results thus demonstrate both a conceptually new cell architecture that is broadly applicable to many aqueous electrolyte chemistries and a specific high-performance example thereof.

BROADER CONTEXT

Most battery research focuses on active electrode materials and/or electrolytes. This approach, however, neglects key materials that determine the commercial viability of the complete cell, e.g., current collectors and packaging. A “total-device” research perspective is essential for aqueous electrochemical energy storage. Commercialized aqueous secondary batteries operate in alkaline media using nickel current collectors, or in acid using lead current collectors.¹ Lead, however, is heavy, and nickel is corroded in all but basic conditions, making them ill-suited for developing new electrolytes and cell chemistries. Instead, researchers use coin cells, Swagelok® cells, or custom-built cells: setups that scale poorly for practical applications. To address the need for a scalable aqueous platform, we designed a pouch cell with lightweight

carbon/polymer composite film current collectors. The composite is stable over a range of pH and compatible with virtually any aqueous electrolyte chemistry. We demonstrate the flexibility of the design by building a prototype zinc-bromine battery. The 4-cell stack matches the voltage range of a 6 V Pb-acid battery with a comparable energy density, but much higher power and cycling stability. The technology has potential applications in automotive engine start-stop, uninterruptible power supplies, hybrid electric vehicles, electrical grid storage, and heavy machinery.

INTRODUCTION

Aqueous electrochemical energy storage is currently under intense investigation and development due to its promise of low-cost, environmentally-friendly, high-power, and safe operation.²⁻⁹ Despite recent advances with electrode materials and electrolytes, however, translations of new systems into practical applications are scarce and the existing commercialized aqueous technologies (NiMH, NiCd, NiZn, and Pb-acid) have not been displaced.¹ This lack of commercialization is largely due to incompatibilities with current aqueous cell designs and the cost and technical difficulties in transitioning from lab-scale cell architectures to large-scale manufacturable devices. It is thus important not only to improve active materials, but also to develop strategies that encompass the design of the entire cell and its passive components. The current collector (CC), in particular, is an essential, but often overlooked, component of all electrochemical energy storage devices that has a significant impact on the viability of upscaling.

Current collectors provide mechanical support for the active materials in the electrode and a path for electrons to travel to and from the device terminals. A CC designed for

commercial high-power aqueous devices must be low-cost, electrically conductive, mechanically robust, and (electro)chemically stable in the electrolyte under a wide range of working potentials. Additionally, CCs must be thin and lightweight to fulfill volume and weight goals. Designing or selecting CCs that simultaneously meet all of these critical requirements is challenging. Metal foils, for example, provide high electronic conductivity, but aqueous electrolytes corrode most metals, limiting practical choices to stainless steel, nickel, or titanium.^{3,10–13} Even these metals/alloys are unstable in acidic media, limiting their use to neutral-pH and alkaline chemistries.

Carbon, in principle, has several advantages over metal as a current collector. Carbon allotropes are stable over a wider range of electrolytes,¹⁴ and typically have a lower contact resistance with electrode materials due to the lack of a passivating oxide layer.¹⁵ Carbon suppresses hydrogen and oxygen evolution due to large kinetic overpotentials, which effectively widen the electrochemical stability window in aqueous electrolytes.⁵ Consequently, the use of carbon as a current collector has been well explored. Expanded graphite foil has been shown to be a suitable current collector for aqueous electrochemical energy storage, but one drawback is its porous structure, which makes it permeable to electrolyte.^{6,16–18} Carbon fiber and carbon nanotube papers and mats have also been used, but are again porous, fragile, and too resistive for practical application.^{3,17} In flow batteries and fuel cells, rigid graphite or carbon/polymer composite plates are commonly employed as CCs, but these massive components are often responsible for the majority of the cost, weight, and volume of the stack, making them unattractive for use in compact, portable (non-flow) cells.^{19,20} Likewise, although pyrolytic graphite is resistant to corrosive electrolytes, it is not mechanically tough and its high cost rules it out as a CC candidate for mass production.²¹

Here we report the use of a thin (70 μm) carbon/polymer composite film as a current collector material. Although many different carbon/polymer films can be produced, we focus on a carbon black/polyethylene composite (CBPE).²² This material is commercially available (mass-produced for antistatic packaging), low-cost, and lightweight (see SI for detailed properties). We systematically investigate and demonstrate that CBPE exhibits a wide electrochemical stability window in a variety of aqueous electrolytes; however, its low conductivity prevents its use as a CC in a conventional cell architecture. To address this critical drawback, we used a *bipolar pouch-cell architecture* in which the current flows through-plane instead of in-plane, shortening the distance the current must travel through the CBPE CC, and hence lowering the effective resistance. This configuration permits one to choose a current collector material with a higher resistivity than previously, thus solving the low electrical conductivity issue of using CBPE. Further, the flexible, electrolyte-impermeable, and heat-sealable CBPE composite serves simultaneously as the cell packaging and seal in addition to its role as current collector, enabling the simple construction of stacked pouch cells with shared bipolar CCs. Compared to previous work on carbon/polymer composite CCs, this design is advantageous because it uses thinner materials, simplifies construction/sealing, and does not require metallization or modification of the material.^{23–25}

To test this concept for use in aqueous electrochemical energy storage, we construct non-flow zinc-bromine batteries. These devices show that the system operates effectively under challenging conditions that combine a corrosive and acidic electrolyte with a wide range of operating voltages. These cells incorporate tetrabutylammonium bromide and activated carbon to address the problematic low power densities, poor Coulombic efficiency, and fast self-discharge rates typical of zinc-bromine batteries.^{26,27} We achieve a cell-level energy density of 50 W h L^{-1}

at a 10 C rate (0.5 kW L^{-1}), with less than 1% capacity loss over 500 cycles. Additionally, we report a large 4-cell stack to illustrate the scalability of the pouch cells without sacrificing performance. The resulting device employs three bipolar CCs, operates in the range of 6-7 V, and has an internal self-balancing mechanism that protects the individual cells in the stack from overcharging damage.

RESULTS AND DISCUSSION

Electrochemical stability of current collectors

A broadly applicable current collector must withstand wide anodic and cathodic polarization and resist corrosion in neutral, acidic, and basic pH electrolytes. The corrosion protection of metals such as stainless steel (SS), nickel, and titanium derives from the formation of surface passivation layers. Passivating metal oxide films, however, are electrically insulating, resulting in high interfacial contact resistance between the electrode and current collector.¹⁵ Even in neutral-pH electrolytes, passivated metals are susceptible to pitting corrosion under anodic bias when aggressive anions such as halide salts or sulfates are present.^{10,28,29} In other cases the current collector can be stable and still cause cell performance degradation via electrolyte decomposition, especially with metals such as platinum and gold that facilitate water splitting.⁵

We investigated the electrochemical stability window of CBPE and compared it to SS, Ni, and Ti metal current collectors for aqueous devices using linear sweep voltammetry (Fig. 1). The electrolytes tested were sodium sulfate, sulfuric acid, potassium hydroxide, and sodium chloride, representing neutral, acidic, basic, and pitting conditions, respectively. The CBPE material shows the highest overpotential for hydrogen evolution in all electrolytes tested on the cathodic sweep, indicating wide compatibility with different pH values and electrolyte

conditions. On the anodic sweeps, CBPE also exhibits much higher stability than Ni and SS. In sulfuric acid (1 M H_2SO_4), for example, Ni corrodes immediately, and although SS shows some corrosion resistance, its stability limit is almost 1 V lower than that of CBPE. With chloride present in the electrolyte (1 M NaCl), CBPE is stable to ~ 1.4 V vs. Ag/AgCl, beyond the potential at which Cl^- is oxidized to chlorine gas (Cl_2). In contrast, Ni and SS are susceptible to pitting corrosion under anodic bias with the halide salt present. Titanium appears to have even higher stability on the anodic sweep in some electrolytes, but this electrochemical behavior is likely due to the formation of an oxide passivation layer that would result in a high contact resistance at the electrode/CC interface.

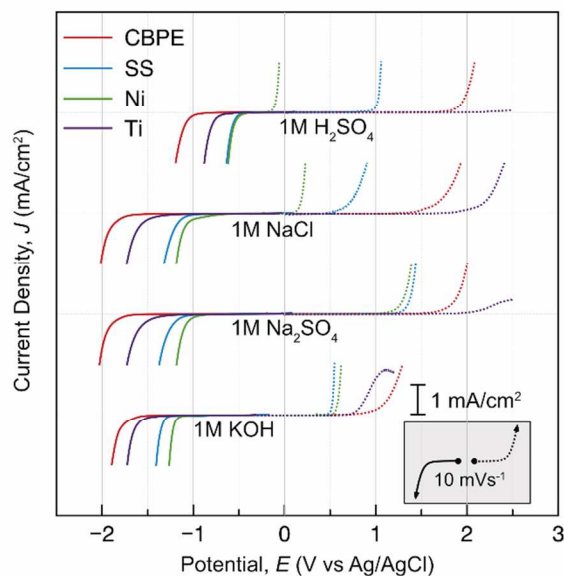


Fig. 1 Relative electrochemical stability of candidate current collectors in different aqueous electrolytes. Linear sweep voltammetry of stainless steel (SS), nickel, titanium, and carbon black/polyethylene composite film (CBPE) reveals the relative stability window of these materials in 1 M H_2SO_4 , 1 M Na_2SO_4 , 1 M NaCl, and 1 M KOH electrolytes. The flat region in the center of each sweep represents the electrochemical stability window. On the cathodic sweep an increase in current represents hydrogen evolution, and on the anodic sweep an increase in current represents oxygen evolution, corrosion, or anodization.

In many aqueous electrolytes, cells can be charged beyond the thermodynamic 1.23 V stability window of water to increase power and energy, provided appropriate current collectors and electrodes are used.^{29–32} The electroanalytical study above shows that the CBPE material provides a stability window of ca. 2.5 – 3 V in a variety of aqueous electrolytes and pH values. Other materials have much narrower stability windows, suggesting that it is the CC that limits the electrochemical stability window in many cases rather than the electrolyte. The wider stability window with the CBPE composite, therefore, provides an opportunity to extend operating voltages for further development of new electrodes and electrolytes without limitations from the current collector.

Electrical conductivity – monopolar versus bipolar cell design

Current collectors (CCs) must have high electrical conductivity to minimize cell resistance. One often-cited advantage of aqueous rechargeable batteries and electrochemical capacitors is the large power density (viz., cycling on the order of 100 C or 10 A g⁻¹, respectively) that is possible due to the high ionic conductivity of aqueous electrolytes.^{2,33} While these high rates are achievable in coin-type cells, performance decreases when these systems are scaled up and the cell design becomes dependent on CC resistivity/conductivity. In this work, we compare three metallic CCs (stainless steel, nickel, and titanium) and three carbon-based CCs (expanded graphite, pyrolytic graphite, and CBPE) and analyze which are suitable for different aqueous cell designs and sizes. As a reference, the resistivities, ρ , of these materials are summarized in Table S1 and shown graphically in Fig. 2c.

A fundamental challenge with a typical monopolar cell architecture for high-power devices is that current flows in-plane in the current collector through a small cross-sectional area (we refer this platform as a “traditional” or “conventional” cell architecture throughout). As the cell height, L , increases, a correspondingly larger current must flow over longer distances through the same cross-sectional area, A , significantly increasing ohmic losses (Fig. 2a). These losses force one to use thicker current collectors in larger cells to decrease their resistance, R , which is inversely proportional to A . Fig. 2c illustrates the maximum allowed resistivity (and the equivalent minimum required conductivity) of a CC material in a hypothetical high-power device as a function of cell size (i.e. height in the model here), for several CC thicknesses. The calculation is performed for a case that limits the CC contribution to the IR drop to 100 mV at a current density of $\pm 100 \text{ mA cm}^{-2}$ (Fig. S1 and calculation details in SI). This requirement ensures that during high-rate charge and discharge of a 1 V cell, for example, less than 10% of the total energy is lost to CC ohmic I^2R losses as heat. Under these conditions, in-plane current flow in the conventional cell configuration puts a significant constraint on the allowed resistivity of the CC materials (the CC materials from Table S1 are added to Fig. 2c for comparison). For the high-power conditions evaluated, it is apparent that expanded graphite (EG), for example, is only suitable for small cells (cell size $< 2.5 \text{ cm}$). In larger cells, much thicker EG sheets would be needed, degrading the cell-level volumetric and gravimetric power and energy performance. Metals have better conductivity than EG and can therefore accommodate larger cell sizes before the CCs become prohibitively thick. Although it is stable and corrosion-resistant, CBPE is unusable in a conventional cell format due to its large resistivity, which is ~ 5 orders of magnitude too high.

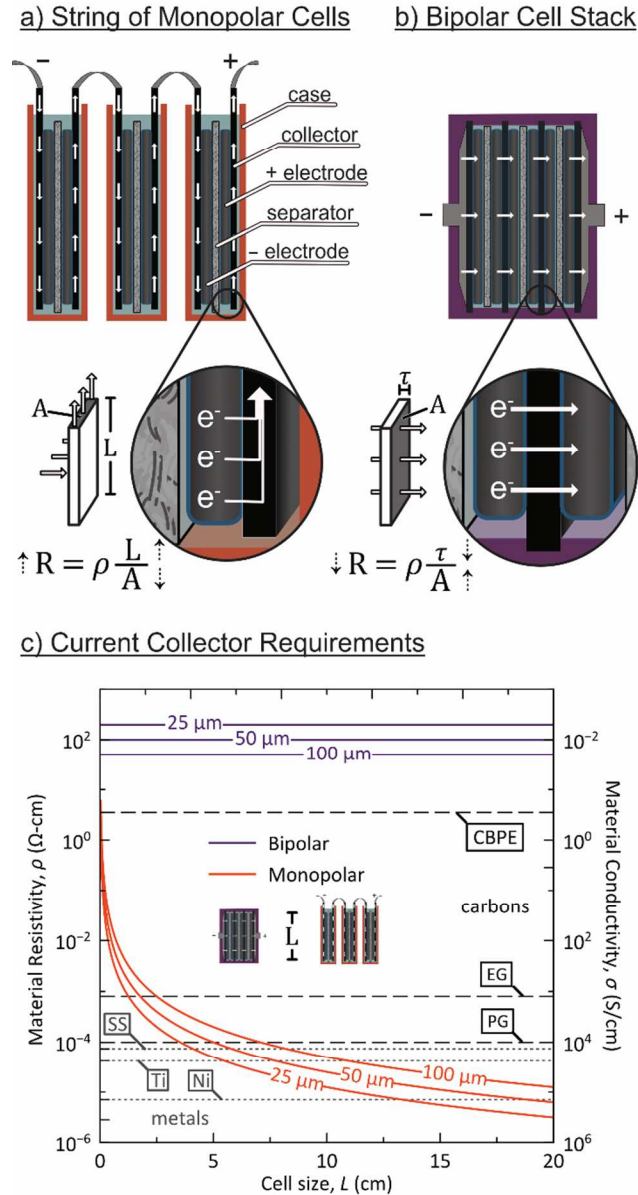


Fig. 2 Monopolar and bipolar cell architectures. (a) Series string of three monopolar cells showing typical cell components. Current flows in the plane of the current collector to external tabs which connect the cells in the pack. The equation illustrates that the combined resistance, R , from the two CCs in each cell is high when current travels long distances through a small area, A . (b) Three equivalent cells with the same components and dimensions arranged in a bipolar cell stack, where current flows directly between cells by traveling in the through-plane direction of a shared bipolar current collector. For cells with the same current collector material, the resistance will be lower in the bipolar configuration due to the shorter path length, τ , and larger cross-sectional area, A . (c) Maximum acceptable resistivity versus cell size (L) shown for 25-, 50-, and

100- μm -thick CCs for monopolar cells (orange curves) and bipolar cells (purple lines). Actual resistivity values for metal CC materials (dotted gray lines) and carbon CC materials (dashed black lines) are included for comparison. The calculations assume perfect tabbing and uniform current density with the constraint that CC IR drop is ≤ 100 mV at ± 100 mA cm^{-2} (CC IR drop is from the internal resistance due to current collectors only, and neglects contributions from electrodes, electrolyte, and contact resistance). EG = expanded graphite, PG = pyrolytic graphite, and SS = 316L stainless steel.

To circumvent the insufficient electrical conductivity of CBPE in a conventional cell architecture, a bipolar cell design can be used. In this configuration, current flows through-plane over a distance of less than 100 μm instead of in-plane over a distance of centimeters, allowing for the current collector material to have higher resistivity (Fig. 2b). Because CCs are shared between adjacent cells in a bipolar cell stack, a single CC serves as the positive current collector for one cell and the negative CC for its neighbor. This arrangement presents a technical challenge by requiring the CC material to be stable under both anodic and cathodic bias extremes, and thus excludes many CC materials from use in a bipolar cell architecture. Importantly, the wide electrochemical stability window of CBPE satisfies this criterion, making it an ideal candidate for bipolar cells.

Repeating the CC resistivity calculations for bipolar architectures (purple lines in Fig. 2c) shows that the resistivity of CBPE (3.5 $\Omega\text{-cm}$) is significantly lower than the required values of 200 or 50 $\Omega\text{-cm}$ for 25 or 100 μm -thick bipolar CCs, respectively (example calculation in the SI). This confirms that the short path length, τ , traveled by current in the bipolar cell design as well as the larger cross-sectional area, A , solve the problems associated with CBPE's low electrical conductivity (Fig. 2b). An added benefit of the bipolar configuration is that the current density is uniform at all points in the cell, so the current collector requirements stay constant as

the cell scales to larger sizes. This uniform current density also eliminates voltage gradients between the tabbing point and the opposite edge of the current collector found in a monopolar design, producing uniform charging, discharging, and heat generation across the entire electrode.

Areal cost, mass, and volume

In electrochemical energy storage, cost, mass, and volume must be minimized in order to optimize an overall figure of merit for the entire system. This requirement applies to all cell components, including current collectors, and not just to active materials.^{6,34} For example, if an electrode has a mass loading on the order of 10 mg cm^{-2} and a current collector also has an areal mass of 10 mg cm^{-2} , the effective gravimetric performance metrics of the electrode are reduced by 50% (or by 33% for double-sided coating), before considering further performance reductions from the mass of electrolyte and other passive cell components. Bipolar designs decouple some of the current collector requirements and tradeoffs. Unlike the behavior in a conventional monopolar cell architecture, thinner CC materials *decrease* ohmic losses in bipolar cells, as discussed in the previous section and illustrated in Fig. 2c. Thinner CC materials increase cell-level volumetric and gravimetric performance and decrease material costs (except for extremely thin specialty materials, where processing costs exceed the savings from using less total material). This relationship means that for any cell size, the selection of bipolar CC material should be based on the minimum commercially available thickness.

The thickness, areal cost, and areal mass of the thinnest mass-produced form found on the market for the three metallic and three carbon-based CCs are discussed in the SI and summarized in Table S1 and Fig. S2. The different materials each have unique disadvantages. Expanded graphite, for example, is thick relative to the other materials at $130 \mu\text{m}$. Stainless steel and nickel

are heavy, with areal mass greater than 20 mg cm^{-2} . Finally, titanium and pyrolytic graphite are expensive, with areal costs of approximately $\$5\text{-}\10 m^{-2} . Of the materials investigated, only the CPBE composite offers both low areal cost and mass ($\$1.6 \text{ m}^{-2}$ and 8.1 mg cm^{-2} , respectively) at an acceptable thickness ($70 \text{ }\mu\text{m}$). We note that the thinness of the CBPE is critical for non-flow battery applications, and distinguishes it from the carbon-polymer composite plates used in flow batteries, which have 20-50 times higher areal cost and mass due to their increased thickness (1-5 mm) and the fact that they are produced with compression or injection molding rather than roll-to-roll processing.³⁵⁻³⁷ The drawback of CBPE is its low electrical conductivity, but when incorporated as a thin film in a bipolar configuration it becomes an ideal CC candidate for low-cost, high-performance aqueous electrochemical energy storage.

Electrolyte permeability

After low thickness, cost, electrical resistance, and mass, the final requirement of a bipolar CC material is low electrolyte permeability. If the film is permeable to the electrolyte, leakage current carried by the redox electrolyte would flow between adjacent cells. Electrolyte could also escape from the device. To test the permeability of CBPE, a piece of the film was placed in the center of an H-cell to separate pure water on one side from an aqueous 1 M HBr solution on the other. After 72 h, no pH decrease was measured in the water chamber, indicating negligible crossover of HBr across the CBPE film (Table S2 and Fig. S3). In contrast, repeating the experiment with a $130 \text{ }\mu\text{m}$ -thick sheet of expanded graphite showed a gradual decrease in the pH of the water that corresponds to a high HBr permeability.

Heat-sealed bipolar pouch cells

Another key property of the CBPE material is that the thermoplastic polyethylene in the composite is both flexible and heat sealable. Taking advantage of all of these properties for device engineering, we investigated both individual pouch cells (single CBPE pouch) and stacked bipolar pouch cells (stacked CBPE pouch) where this single composite material serves multiple functions as the cell packaging, current collector, and seal. This concept is illustrated in Fig. 3a, where the cross-sectional schematic and exploded views show how the CBPE material is directly fused with a polyethylene plastic spacer after assembly, encapsulating a cell stack in a sealed pouch. With both the spacer and CBPE being flexible and heat-sealable, alignment and cell construction are straightforward, and the design can be extended to different cell sizes and electrode geometries.

For a single stand-alone cell (Fig. 3a), the impermeable CBPE CCs mainly serve the purpose of protecting metallic endplates from the corrosive aqueous electrolyte. The additional advantages of the design come from its stackable nature, where the total voltage for an n -cell stack equals $n \times E_{\text{cell}}$ (Fig. 3b). In this configuration, the CBPE films shared between adjacent cells function as true bipolar CCs, and the weight, volume, and cost of each are effectively halved relative to that of a single, stand-alone cell. Similarly, the weight, volume and cost of the single pair of endplates is divided among all the cells in the stack. With a heat-sealed, bipolar pouch architecture, the CBPE composite therefore attains a favorable combination of high electrochemical stability, sufficient conductivity, and low cost and weight. In addition, because commercial heat sealers are widely available, CBPE is mass-produced, and the plastic spacers are cut from inexpensive polyethylene, this fabrication process and device architecture can be easily applied to a wide range of aqueous electrochemical energy storage technologies.

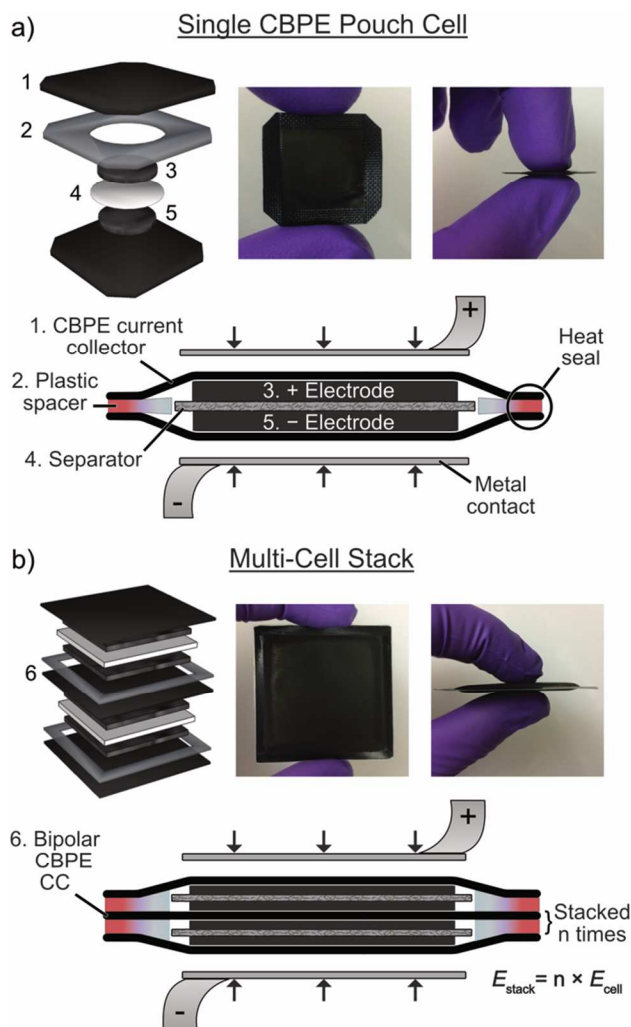
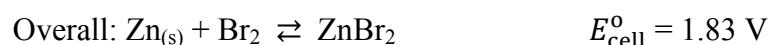
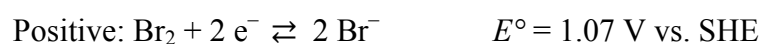
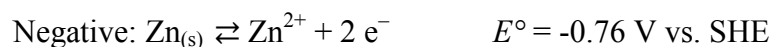


Fig. 3 Single and stacked pouch cells. (a) Exploded view, cross-sectional view, and photographs of a single pouch cell. The cell stack, comprised of freestanding electrodes and a separator, is placed between two CBPE current collectors and surrounded by an insulating plastic spacer. The current collectors are heat-sealed to either side of the spacer to seal the cell. (b) Exploded view and photographs of a larger bipolar pouch with two cells in series and a cross-sectional view of an n -cell bipolar pouch. The photographs in (a) are of a single small pouch cell with round, 11-mm-diameter (300- μm -thick) freestanding electrodes while the photographs in (b) show a larger, bipolar pouch containing two cells in series, each with a pair of square 4 cm \times 4 cm (450- μm -thick) freestanding electrodes. The pouch cells are metal-free. Any metal used externally as stack endplates is protected from corrosion as the electrolytes are contained by the CBPE material.

Demonstrating CBPE pouch cells with a zinc bromine battery

In order to test the utility of pouch cells with CBPE current collectors (CBPE pouch cells) in a demanding application with aggressive aqueous electrolytes, we built aqueous rechargeable batteries with zinc-bromide electrolyte. The battery's basic electrochemistry is summarized below:¹⁹



At the negative electrode, zinc has a reduction potential of -0.76 V vs. SHE at its acidic operating range of pH 1 – pH 3.5. This reduction potential is outside of the thermodynamic stability window of water, but zinc possesses a large overpotential for hydrogen gas evolution, minimizing electrolyte decomposition.²⁶ At the positive electrode, oxidation of bromide to bromine occurs at 1.07 V vs. SHE to give an overall cell voltage of 1.83 V for ZnBr₂ batteries, higher than any commercialized aqueous battery systems with the exception of Pb-acid batteries (ca. 2.1 V).³⁸ This combination of the corrosive bromide anion, an acidic pH, and a wide operating voltage provides a challenging environment not compatible with cell designs that use metallic current collectors, making the zinc-bromine chemistry a good candidate for testing the CBPE pouch-cell platform.

One challenge in the design of (non-flow) zinc bromine pouch cells is the low Coulombic efficiency and fast self-discharge caused by the cross-diffusion of Br₃⁻, which readily forms from Br₂ in aqueous electrolytes containing Br⁻ anions.^{39,40} We previously found that tetrabutylammonium bromide (TBABr) reversibly complexes Br₃⁻ in a solid phase, [TBA⁺ · Br₃⁻]_(s), preventing its diffusion across the cell.⁴¹ However, TBABr is not soluble in zinc bromide

electrolyte because bromozincate anions, $[\text{ZnBr}_4]^{2-}$, readily precipitate as an insoluble complex with TBA^+ , preventing *ex situ* preparation of $\text{ZnBr}_2/\text{TBABr}$ electrolyte.^{42–45} To solve this problem, the activated carbon positive electrode is pre-soaked in a TBABr solution to pre-adsorb this Br_3^- complexing agent at the surface. Next, the electrode is contacted with a paper separator containing zinc-bromide electrolyte and assembled into a cell. This procedure ensures that when a $\text{TBA}/\text{bromozincate}$ complex precipitates, both the complex and the TBA^+ it contains are retained in the high-surface-area pores of the electrode (Fig. S4). After preparing the cell stack, the full assembly is heat-sealed into a single CBPE pouch cell (Figs. S5 and S6; experimental details in the SI). When the full $\text{ZnBr}_2/\text{TBABr}$ cell charges, Br^- is oxidized to Br_3^- at the positive electrode, which complexes with pre-adsorbed TBA^+ and forms a solid at the electrode surface. For the negative electrode, zinc is plated directly from the electrolyte as a solid metal deposit on the CBPE current collector (cyclic voltammetry in Fig. S7). Both of these processes are reversed upon discharge of the cell (Fig. 4a).

The solid complexation of Br_3^- by TBA^+ significantly slowed self-discharge compared to a ZnBr_2 cell without TBABr , increasing energy retention from 12% remaining after 6 h at open circuit without TBABr to 75% remaining when TBABr is present (Fig. 4b), without using costly ion-exchange-membrane separators. Further, this operating mechanism improves the Coulombic efficiency at a 1 A g^{-1} rate from 92% to 99%. It is, however, possible that a small amount of pre-adsorbed TBABr will diffuse throughout the cell after assembly leading to performance degradation. To determine the extent of performance deterioration associated with loss/migration of TBABr from the positive electrode, self-discharge tests were performed on a cell before and after 10 days of operation. The energy retention after 6 h at open-circuit is 73% before this extended cycling and 72% afterwards; the similarity of the self-discharge rate indicates that the

TBABr is not significantly lost from the positive electrode over this time scale and continues to effectively complex Br_3^- .

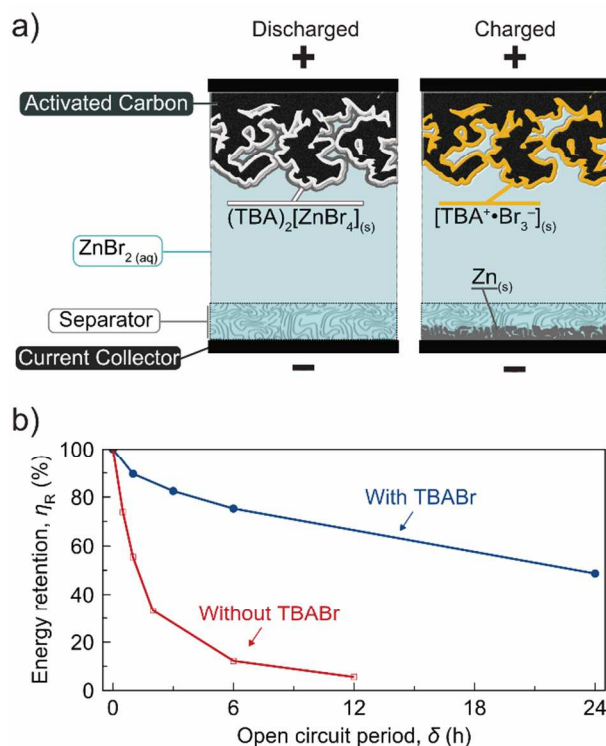


Fig. 4 Zinc-bromine cell charge/discharge mechanism. (a) The $\text{ZnBr}_2/\text{TBABr}$ cell is assembled in the discharged state (left). With this electrolyte chemistry, zinc is reversibly plated onto the CBPE CC as zinc metal at the negative electrode as the cell charges (right). The electrolyte contains a polyethylene glycol additive to minimize zinc dendrite formation (details in the SI).⁴⁶ At the positive electrode, bromide is reversibly oxidized to tribromide and complexed into an insoluble solid with TBA^+ . These processes then reverse on discharge. The electrolyte volume is exaggerated in the schematic. In actual cells, the activated carbon electrode touches the separator and electrolyte only resides in the porous separator and electrode. (b) Self-discharge is measured with and without TBABr present in the cell. The fraction of the initial discharge energy retained after different periods at open circuit is much higher for cells with TBA^+ complexing agent than for equivalent cells without complexing agent.

In order to quantify performance, the $\text{ZnBr}_2/\text{TBABr}$ cells were charged by galvanostatic cycling at 1 A g^{-1} (normalized to the dry mass of the activated-carbon positive electrode) to a capacity of 100 mA h g^{-1} , and discharged to 1 V . A typical galvanostatic charge/discharge (GCD) profile, shown in Fig. 5a, has a low IR -drop and a flat charging plateau, reaching almost 1.8 V on the charge and having an average discharge voltage of more than 1.6 V . Long term cycling shows negligible capacity fading over 2000 cycles with a capacity of 100 mA h g^{-1} and an additional 500 cycles with a capacity of 150 mA h g^{-1} (Fig. 5b). GCD profiles of the 200th and 2000th cycle are shown in Fig. S8; no significant difference in the GCD profiles is observed, consistent with excellent cycling stability.

Additional stability tests were performed to determine how the cell responds to being held at high states of charge or left fully discharged for long periods of time.^{47,48} A cell was held at 1.75 V for 50 h, which corresponds to significant overcharging (the discharge capacity after the voltage hold was 228 mA h g^{-1}). During this voltage hold there was a large average leakage current of 1.4 mA cm^{-2} . When normal cycling to the 100 mA h g^{-1} capacity limit resumed, the specific discharge energy decreased by 3.5 % and the IR -drop increased by 80% (Fig. S9a). This decrease in performance was partially, but not fully, reversed upon continued cycling. In a second test, the cell was held at 1.7 V for 100 h (Fig. S9b). In this case the average leakage current was only $84 \mu\text{A cm}^{-2}$, the discharge capacity after the hold was 107 mA h g^{-1} , and the GCD profile exhibited little change relative to its shape before the 1.7 V hold. Finally, the cell was left fully discharged for 1 week, and then cycled again (Fig. S9c). After this rest, the first cycle exhibited lower Coulombic efficiency (82 %), but the cell exhibited performance equivalent to that before the rest after several cycles.

To measure energy-power performance and various performance efficiencies, a series of charge/discharge rate tests was performed from 0.1 A g^{-1} to 2 A g^{-1} (1 C to 20 C) (Fig. 5c). At the most efficient conditions (1 C rate), a round-trip energy efficiency of 93% is achieved. Charging was limited to 2 A g^{-1} (20 C) or less to prevent the formation of zinc dendrites, but discharge can occur at much higher rates.⁴⁶ Therefore, additional discharge rate tests were performed where the cell was charged only at a single rate of 1 A g^{-1} (10 C) and discharged at different rates of 1 A g^{-1} to 12 A g^{-1} (10 C to 120 C). The GCD profiles from these tests are shown in Fig. S12. The (gravimetric) specific energy and power values in Fig. 5 are normalized only to the mass of the activated-carbon electrode, which has a mass loading of 12.5 mg cm^{-2} , and the (volumetric) energy and power densities are normalized to the full volume of the cell stack (the 1 cm^2 footprint of the positive electrode multiplied by the total combined thickness of the electrode, separator, and CBPE CCs – see SI for details). These energy density and power density values for the $\text{ZnBr}_2/\text{TBABr}$ cells are summarized on the Ragone plot in Fig. 5d. The 50 Wh L^{-1} energy density is lower than the typical zinc-bromine redox flow battery (70 Wh L^{-1}), but the power density is significantly higher ($1\text{-}2 \text{ kW L}^{-1}$ versus 0.1 kW L^{-1}).⁴⁹ This high power is possible because the high-surface-area activated carbon positive electrode helps to overcome the slow kinetics of the bromide redox reactions and the thin cell stack shortens diffusion distances in the electrolyte.³⁸

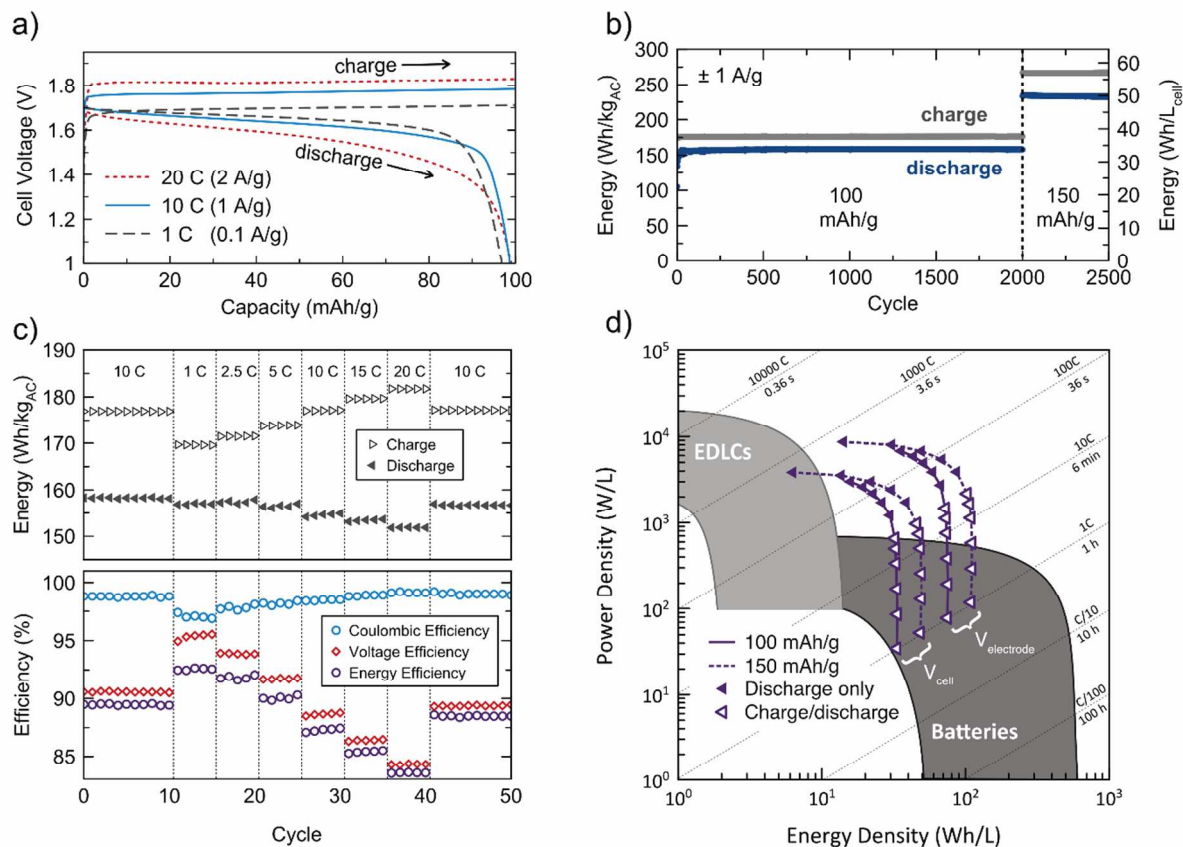


Fig. 5 Electrochemical performance data for a ZnBr₂/TBABr CPBE pouch cell. (a) Typical GCD profiles at different charge/discharge rates. The resulting flat charge/discharge plateaus are in accordance with characteristic zinc-bromine cell chemistry (see Fig. S6 for details of the testing setup). (b) Cycling stability showing charge and discharge energy at a rate of $\pm 1 \text{ A g}^{-1}$ charged to 100 mA h g^{-1} for 2000 cycles and then to 150 mA h g^{-1} for an additional 500 cycles. Energies are normalized to the mass of the activated carbon electrode (left axis) and to the full cell volume (right axis), which includes the electrode, separator, and CBPE CCs. (c) Charge and discharge energy as well as Coulombic, voltage, and energy efficiency (as precisely defined in the SI) at different rates for a cell charged to a capacity of 100 mA h g^{-1} . (d) Ragone plot indicating energy and power density for a cell charging to a capacity of 100 mA h g^{-1} (solid line) or 150 mA h g^{-1} (dashed line). The normalization is shown for the electrode volume only

($V_{\text{electrode}}$) and for the full cell volume (V_{cell}). Open triangles indicate points where the charge and discharge were performed at the same rate (1 C to 20 C) while solid triangles indicate points where charging was limited to 10 C and different high-rate discharges were performed (up to 120 C). Cell-level performance ranges for secondary batteries and electric double layer capacitors (EDLCs) are included for reference. Additional electrochemical performance data for a 150 mA h g⁻¹ capacity limit can be found in Fig. S10, and two-electrode cyclic voltammetry is shown in Fig. S11.

Construction of scaled, bipolar pouch cell stacks

Encouraged by the stable cycling performance of pouch cells with aggressive ZnBr₂ electrolyte in the single-cell format, we turned our attention towards the development of a bipolar stack. A stacked system has the benefit of reaching the high voltages needed for practical applications but is more challenging to fabricate. A bipolar pouch comprised of four cells stacked in series was constructed using the same ZnBr₂/TBABr chemistry from the individual pouch cells (Fig. 6a). The cell stack operates over a voltage range of 6-7 V, and the GCD profile has the same characteristics as that of a single, smaller cell (Fig. 6b). Although the scaled, stacked system is more complex than individual cells and contains 25 times more active electrode material, specific energy is unchanged and long-term cycling again shows negligible capacity fading over 1000 cycles with a capacity of 100 mA h g⁻¹ and an additional 500 cycles with a capacity of 150 mA h g⁻¹ (Fig. 6c). The prototype was then connected to a pair of 3 W blue LEDs to show a practical demonstration that requires a much higher voltage and current than a single small test cell can provide (Fig. 6d).

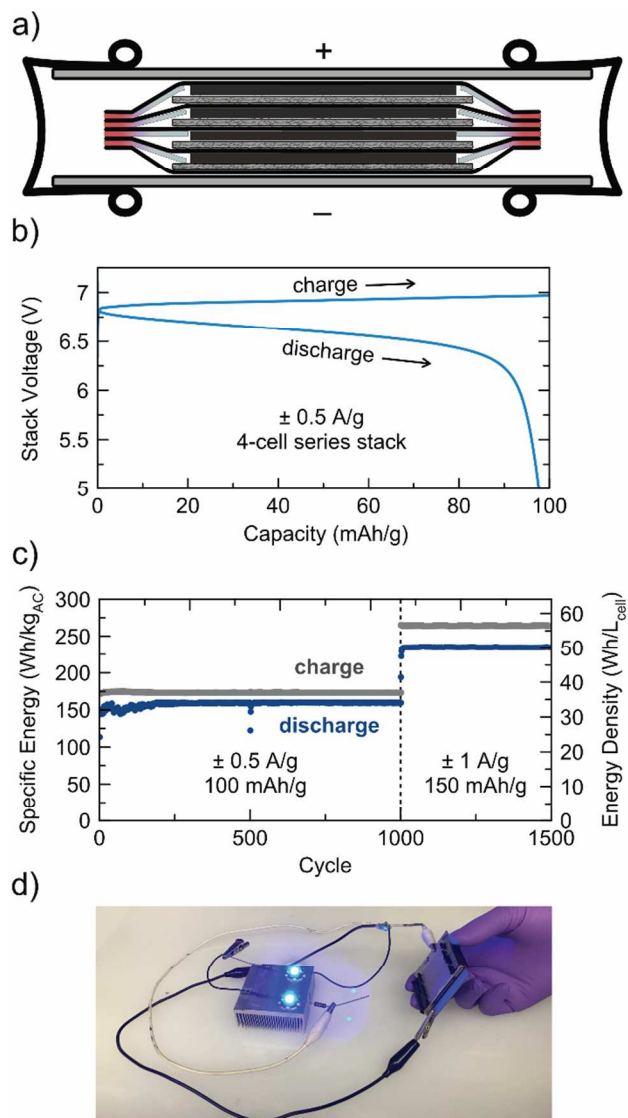


Fig. 6 Performance of a scaled, bipolar pouch. (a) Schematic (not to scale) of a four-cell bipolar stack with shared CBPE CCs, $2.5 \text{ cm} \times 2.5 \text{ cm}$ ($265\text{-}\mu\text{m}$ -thick) activated carbon electrodes, and $\text{ZnBr}_2/\text{TBABr}$ electrolyte. The cell stack is compressed by four binder clips between two thin titanium plates (see Fig. S5 for fabrication details). (b) Typical GCD profile at 0.5 A g^{-1} (normalized to a single electrode). (c) Cycling stability at a rate of $\pm 0.5 \text{ A g}^{-1}$ (5 C) charged to a capacity of 100 mA h g^{-1} for 2000 cycles and then at a rate of $\pm 1 \text{ A g}^{-1}$ (10 C) charged to a capacity of 150 mA h g^{-1} for an additional 500 cycles. Energies are normalized to the mass of all four activated-carbon electrodes (left axis) and to the full stack volume (right axis), which includes the electrodes, separators, and CBPE CCs. We note that the cell rested for

several days after cycle 500 and cycle 1000. (d) Photograph showing the prototype running a series-connected pair of 3 W blue LEDs.

One issue faced by series stacks of traditional zinc-bromine flow batteries is shunt currents and slow hydrogen evolution.^{26,50} This problem arises because the whole stack shares a common electrolyte volume and the individual cells are not electrochemically isolated.³⁶ This architecture allows strong electric fields to develop near electrolyte inlets and outlets, encouraging hydrogen production. In the bipolar pouch cell stack reported here, however, there is no flowing electrolyte and the individual cells are completely isolated. Additionally, as discussed in the next section, there is excess zinc bromide in the electrolyte and a mechanism to prevent overcharging of individual cells in the stack. These factors will limit parasitic hydrogen evolution.⁵¹ The stable cycling performance and lack of swelling of the pouches confirm that any hydrogen production is minimal.

Another issue encountered by traditional zinc-bromine flow batteries is the attack by bromine and tribromide in the electrolyte on the carbon-polymer composite plates.⁴⁹ The CBPE film is also susceptible to this corrosion mechanism. The SEM micrographs in Fig. S13 show damage to the composite surface after 16 days soaking in pure Br₂. In practical cell operation, bromine complexing agents slow this attack by reducing free bromine concentration in the cell.⁴¹ Although no significant performance degradation was observed over months of cycling, slow attack by tribromide and/or bromine on the CBPE is possible and long-term testing on the order of years is needed. To look for early signs of damage to the CBPE composite, a cell was disassembled after 1500 cycles and the surface of the positive CBPE CC was imaged (Fig. S14). The material looks very similar to its pristine state before cycling, indicating that any attack on the material is relatively insignificant.

Self-balancing for series-connected pouch cells

The stable cycling of the stacked ZnBr_2 system is notable because it indicates that the cells in the bipolar stack remain balanced, keeping the individual cell voltages and capacities closely matched and within safe levels. In a typical series-connected pack of monopolar cells, the terminals for each cell are exposed and thus individual cells can be separately charged to their correct capacity or voltage in order to balance the pack. In a bipolar stack, however, there is no access to terminals of individual cells, so a cell in the stack is vulnerable to being overcharged or overdischarged, damaging the performance of the entire stack.⁵² This destructive behavior is not observed in the stacked $\text{ZnBr}_2/\text{TBABr}$ cells here because intrinsic self-balancing chemistry occurs. When cells are overcharged and all pre-adsorbed TBA^+ is utilized in solid complexation, excess zinc bromide remains in the electrolyte. Charging thus continues and any additional Br_3^- generated can escape the positive electrode uncomplexed and diffuse across the cell where it is reduced back to Br^- (Fig. 7). This redox “shuttle” effect incrementally lowers Coulombic efficiency (CE) as charging capacity increases (Fig. S15). Overcharged cells will have a lower CE (high leakage current) while undercharged cells will have a higher CE (low leakage current). This redox-shuttle can be utilized as an effective mechanism to prevent overcharging of individual cells and to balance multiple cells connected in series.^{26,53,54} If one cell in a series stack becomes overcharged, the $\text{Br}^-/\text{Br}_3^-$ redox shuttle will temporarily result in a large internal leakage current until the other cells in the stack reach the same fully charged state (with equal leakage current). This built-in self-balancing mechanism is demonstrated experimentally and reported in the SI by cycling two cells connected in series, deliberately overcharging one cell while the other rests, and then reconnecting the cells for continued cycling (Fig. S16).

Monitoring the cells after they are reconnected shows that in less than 50 cycles the GCD profiles re-converge, indicating that the pair has rebalanced. Therefore, this electrochemistry has a built-in mechanism for self-balancing that does not require water splitting (gassing) that would typically be used for a Pb-acid battery, or a battery management system (BMS) that would typically be used for lithium-ion packs. Although this mechanism is specific to the zinc-bromine chemistry, the CBPE bipolar pouch format with other aqueous electrochemical energy storage technologies could utilize similar strategies to balance the individual cells by adding an appropriate redox couple to the electrolyte.⁵²

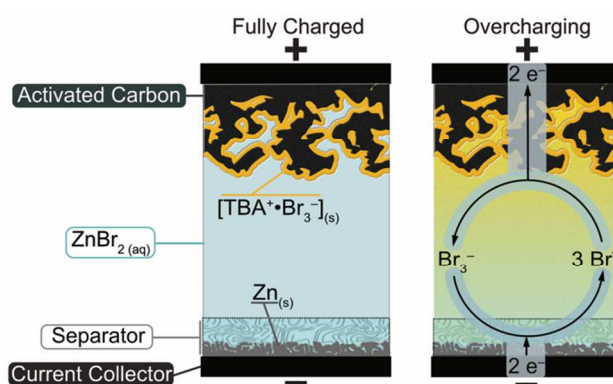


Fig. 7 Built-in self-balancing mechanism to prevent overcharging of ZnBr_2 cells.

Overcharging the ZnBr_2 chemistry causes uncomplexed tribromide to diffuse across the cell, which creates a temporary internal short circuit. This redox shuttle mechanism prevents overcharging damage to individual cells and helps balance multiple cells when they are connected in series.

CONCLUSIONS

The lack of viable cell designs and the need for low-cost, lightweight, and electrochemically stable current collectors are major barriers to implementing high-power aqueous energy-storage technologies. The heat-sealed bipolar pouch cell design with CBPE

current collectors developed here offers a promising platform for constructing high-performance aqueous batteries, supercapacitors, pseudocapacitors, and redox ECs, which helps address this above problem. The electrochemical inertness over a wide range of electrolyte chemistries and the simple assembly with low-cost equipment and consumables make the system attractive for research applications. The pouch cells also use only commercially available materials and are easily modified to accommodate larger electrodes and different geometries, which is important for commercial development. The cell performance could further increase as thinner, stronger, and more conductive carbon/polymer composite films are developed. Additionally, the non-flow $\text{ZnBr}_2/\text{TBABr}$ cells deliver battery-level energy density, supercapacitor-level power density, and long-term cycling stability to provide a high-performance example of the effectiveness of the CBPE pouch cells with a challenging electrolyte.

CONFLICTS OF INTEREST

BE, SJY, JL, XJ, SWB, and GDS are co-inventors on a pending patent application relevant to this work.

ACKNOWLEDGMENTS

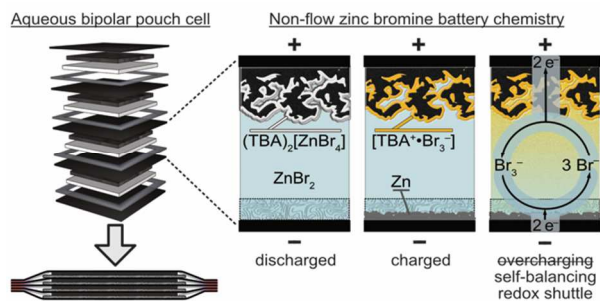
This research was supported by the Advanced Research Projects Agency-Energy (ARPA-E), U.S. Department of Energy (Award No. DE-AR0000344), the Southern California Electrochemical Energy Storage Alliance (SCEESA), and the National Research Foundation of Korea (NRF) grant funded by the Korea government (Ministry of Science, ICT & Future Planning) (NRF-2017R1C1B2005470). S.W.B. acknowledges the Alfred P. Sloan and Dreyfus Foundations for additional support. We are grateful to Prof. Ram Seshadri and Prof. Fred Wudl for discussions regarding this work and to Daniel Lubin and Nicholas Parker for their contributions to the project.

REFERENCES

- 1 K. Nishio and N. Furukawa, in *Handbook of Battery Materials: Second Edition*, Wiley-VCH Verlag, Weinheim, 2011, pp. 27–85.
- 2 H. Kim, J. Hong and K. Park, *Chem. Soc. Rev.*, 2014, **114**, 11788–11827.
- 3 J. Yan, Q. Wang, T. Wei and Z. Fan, *Adv. Energy Mater.*, 2014, **4**, 1300816.
- 4 Y. Liang, Y. Jing, S. Gheytani, K. Lee, P. Liu, A. Facchetti and Y. Yao, *Nat. Mater.*, 2017, **16**, 841–848.
- 5 M. R. Lukatskaya, S. Kota, Z. Lin, M. Q. Zhao, N. Shpigel, M. D. Levi, J. Halim, P. L. Taberna, M. W. Barsoum, P. Simon and Y. Gogotsi, *Nat. Energy*, 2017, **6**, 1–6.
- 6 J. F. Whitacre, T. Wiley, S. Shanbhag, Y. Wenzhuo, A. Mohamed, S. E. Chun, E. Weber, D. Blackwood, E. Lynch-Bell, J. Gulakowski, C. Smith and D. Humphreys, *J. Power Sources*, 2012, **213**, 255–264.
- 7 X. Wu, Y. Qi, J. J. Hong, Z. Li, A. S. Hernandez and X. Ji, *Angew. Chemie - Int. Ed.*, 2017, **56**, 13026–13030.
- 8 S.-E. Chun, B. Evanko, X. Wang, D. Vonlanthen, X. Ji, G. D. Stucky and S. W. Boettcher, *Nat. Commun.*, 2015, **6**, 7818.
- 9 J. Lee, P. Srimuk, S. Fleischmann, M. Zeiger, V. Presser and A. Ridder, *J. Mater. Chem. A*, 2017, **5**, 12520–12527.
- 10 S. Gheytani, Y. Liang, Y. Jing, J. Q. Xu and Y. Yao, *J. Mater. Chem. A*, 2016, **4**, 395–399.
- 11 Y. Yamada, K. Usui, K. Sodeyama, S. Ko, Y. Tateyama and A. Yamada, *Nat. Energy*, 2016, **1**, 1–9.
- 12 X. Zhou, C. Peng and G. Z. Chen, *AIChE J.*, 2012, **58**, 974–983.
- 13 K. C. Ng, S. Zhang, C. Peng and G. Z. Chen, *J. Electrochem. Soc.*, 2009, **156**, A846.
- 14 W. Zuo, R. Li, C. Zhou, Y. Li, J. Xia and J. Liu, *Adv. Sci.*, 2017, **4**, 1600539.
- 15 H.-C. Wu, Y.-P. Lin, E. Lee, W.-T. Lin, J.-K. Hu, H.-C. Chen and N.-L. Wu, *Mater. Chem. Phys.*, 2009, **117**, 294–300.
- 16 N. Blomquist, T. Wells, B. Andres, J. Bäckström, S. Forsberg and H. Olin, *Sci. Rep.*, 2017, **7**, 1–7.
- 17 B. Dyatkin, V. Presser, M. Heon, M. R. Lukatskaya, M. Beidaghi and Y. Gogotsi, *ChemSusChem*, 2013, **6**, 2269–2280.
- 18 B. Ziv, O. Haik, E. Zinigrad, M. D. Levi, D. Aurbach and I. C. Halalay, *J. Electrochem. Soc.*, 2013, **160**, A581–A587.
- 19 J. Noack, N. Roznyatovskaya, T. Herr and P. Fischer, *Angew. Chemie - Int. Ed.*, 2015, **54**, 9776–9809.
- 20 L. Du and S. C. Jana, *J. Power Sources*, 2007, **172**, 734–741.
- 21 P. Han, B. Zhang, C. Huang, L. Gu, H. Li and G. Cui, *Electrochem. commun.*, 2014, **44**, 70–73.
- 22 R. Sengupta, M. Bhattacharya, S. Bandyopadhyay and A. K. Bhowmick, *Prog. Polym. Sci.*, 2011, **36**, 638–670.
- 23 M. Ghaemi, R. Amrollahi, F. Ataherian and M. Z. Kassaei, *J. Power Sources*, 2003, **117**,

- 233–241.
- 24 M. D. Stoller, S. Park, Y. Zhu, J. An and R. S. Ruoff, *Nano Lett.*, 2008, **8**, 3498–502.
- 25 H. Karami, M. F. Mousavi, M. Shamsipur and S. Riahi, *J. Power Sources*, 2006, **154**, 298–307.
- 26 S. Biswas, A. Senju, R. Mohr, T. Hodson, N. Karthikeyan, K. W. Knehr, A. G. Hsieh, X. Yang, B. E. Koel and D. A. Steingart, *Energy Environ. Sci.*, 2017, **10**, 114–120.
- 27 Q. Lai, H. Zhang, X. Li, L. Zhang and Y. Cheng, *J. Power Sources*, 2013, **235**, 1–4.
- 28 F. Béguin, V. Presser, A. Balducci and E. Frackowiak, *Adv. Mater.*, 2014, **26**, 2219–2251.
- 29 P. Ratajczak, K. Jurewicz, P. Skowron, Q. Abbas and F. Béguin, *Electrochim. Acta*, 2014, **130**, 344–350.
- 30 Q. Gao, L. Demarconnay, E. Raymundo-Piñero and F. Béguin, *Energy Environ. Sci.*, 2012, **5**, 9611–9617.
- 31 K. Fic, G. Lota, M. Meller and E. Frackowiak, *Energy Environ. Sci.*, 2012, **5**, 5842–5850.
- 32 L. Zhang, L. Chen, X. Zhou and Z. Liu, *Adv. Energy Mater.*, 2015, **5**, 1–5.
- 33 C. D. Wessells, R. A. Huggins and Y. Cui, *Nat. Commun.*, 2011, **2**, 550.
- 34 Y. Gogotsi and P. Simon, *Science*, 2011, **334**, 917–918.
- 35 C. Minke, T. Hickmann, A. R. Dos Santos, U. Kunz and T. Turek, *J. Power Sources*, 2016, **305**, 182–190.
- 36 P. Leung, X. Li, C. Ponce de León, L. Berlouis, C. T. J. Low and F. C. Walsh, *RSC Adv.*, 2012, **2**, 10125–10156.
- 37 P. Qian, H. Zhang, J. Chen, Y. Wen, Q. Luo, Z. Liu, D. You and B. Yi, *J. Power Sources*, 2008, **175**, 613–620.
- 38 G. P. Rajarathnam and A. M. Vassallo, *The Zinc/Bromine Flow Battery*, SpringerNature, Singapore, 2016.
- 39 P. Singh, K. White and A. J. Parker, *J. Power Sources*, 1983, **10**, 309–318.
- 40 B. Evanko, S. J. Yoo, S.-E. Chun, X. Wang, X. Ji, S. W. Boettcher and G. D. Stucky, *J. Am. Chem. Soc.*, 2016, **138**, 9373–9376.
- 41 S. J. Yoo, B. Evanko, X. Wang, M. Romelczyk, A. Taylor, X. Ji, S. W. Boettcher and G. D. Stucky, *J. Am. Chem. Soc.*, 2017, **139**, 9985–9993.
- 42 M. E. Easton, P. Turner, A. F. Masters and T. Maschmeyer, *RSC Adv.*, 2015, **5**, 83674–83681.
- 43 K. J. Cathro, K. Cedzynska, D. C. Constable and P. M. Hoobin, *J. Power Sources*, 1986, **18**, 349–370.
- 44 P. Trouelan, J. Lefebvre and P. Derollez, *Acta Crystallogr.*, 1985, **41**, 846–850.
- 45 S. V. Rosokha and M. K. Vinakos, *Cryst. Growth Des.*, 2012, **12**, 4149–4156.
- 46 S. J. Banik and R. Akolkar, *J. Electrochem. Soc.*, 2013, **160**, D519–D523.
- 47 P. W. Ruch, D. Cericola, A. Foelske-Schmitz, R. Kötz and A. Wokaun, *Electrochim. Acta*, 2010, **55**, 4412–4420.
- 48 D. Weingarh, A. Foelske-Schmitz and R. Kötz, *J. Power Sources*, 2013, **225**, 84–88.
- 49 P. C. Butler, P. A. Eidler, P. G. Grimes, S. E. Klassen and R. C. Miles, in *Handbook of Batteries*, eds. D. Linden and T. B. Reddy, McGraw-Hill, Ohio, 2001.

- 50 M. Skyllas-Kazacos, M. H. Chakrabarti, S. A. Hajimolana, F. S. Mjalli and M. Saleem, *J. Electrochem. Soc.*, 2011, **158**, R55.
- 51 G. L. Soloveichik, *Chem. Rev.*, 2015, **115**, 11533–11558.
- 52 J. Dahn, J. Jiang, L. Moshurchak, C. Buhrmester and R. L. Wang, *Electrochem. Soc. Interface*, 2005, **14**, 27–31.
- 53 N. S. Choi, Z. Chen, S. A. Freunberger, X. Ji, Y. K. Sun, K. Amine, G. Yushin, L. F. Nazar, J. Cho and P. G. Bruce, *Angew. Chemie - Int. Ed.*, 2012, **51**, 9994–10024.
- 54 K. W. Knehr, S. Biswas and D. A. Steingart, *J. Electrochem. Soc.*, 2017, **164**, A3101–A3108.

TABLE OF CONTENTS GRAPHIC

A platform for testing and scaling aqueous batteries and supercapacitors is demonstrated with a high-power/low-self-discharge zinc-bromine cell chemistry.